

Cooling flows and the entropy of the intragroup medium

Biman B. Nath

Raman Research Institute, Bangalore 560080, India

(biman@rri.res.in)

10 April 2024

ABSTRACT

We study steady, homogeneous and subsonic cooling flows in poor clusters of galaxies in light of the recent proposal that radiative cooling of the intracluster gas can explain the observations of the ‘entropy floor’ and other related X-ray observations. We study a family of cooling flow solutions parameterized by the mass flux rate, and then determine the resulting entropy and the X-ray luminosity. We find that cooling flows with mass flux rates in excess of $1000 M_{\odot}$ per yr are required to explain the observations of entropy and X-ray luminosity. In view of the observed lack of such large flows in rich clusters, our calculations suggest that heating sources are needed, in addition to the effect of radiative cooling, to explain the observations.

Key words: Cosmology: Theory | Galaxies: Intergalactic Medium | Galaxies: clusters: general | X-rays: Galaxies: Clusters

1 INTRODUCTION

Studies of the structure of dark matter in collapsed objects of different masses show a remarkable universality. Numerical simulations have shown that the dark matter density profile has a universal shape (Navarro, Frenk & White 1995). This result provides a framework for the study of the relation between the baryonic and dark matter content of halos. Clusters of different masses, with their large baryonic gas content, are excellent probes for such studies. If the physical properties of the baryonic gas contained in these self-similar potential wells were completely governed by gravity, then the observed properties of the gas would also be scale-free (Kaizer 1986). For example, relation between the gas temperature and the cluster

mass or the X-ray luminosity and the temperature, would be independent of the total mass ($L / M^{2=3}$ and L / T^2 , respectively).

Observations, however, show that in reality such relations deviate from being self-similar, pointing out the importance of non-gravitational processes determining the properties of the baryonic gas. The observed relation between luminosity and temperature steepens from the self-similar expectation of L / T^2 for low temperature clusters (e.g., Markevitch 1998; Allen & Fabian 1998). Also the mass-temperature relation shows deviation from self-similarity (e.g., McCarthy et al. 2002).

It has also been observed that the surface brightness profiles of poor groups (with lower temperatures than richer clusters) are relatively shallow (Ponman et al. 1999), showing that the underlying gas density profile is also shallow. All these observations clearly point towards some physical process which raises the entropy of the gas. Indeed, direct determination of the gas entropy (one defines an 'entropy' $S = T = n_e^{2=3}$ which is the entropy of an ideal gas, stripped of the logarithm and the constant factors) shows the existence of an 'entropy floor', a minimum level of entropy. Lower temperature clusters, therefore, have relatively high entropy gas, compared to the expectations from self-similar models. It has been estimated that this 'entropy floor' corresponds to 100 keV cm^{-2} (Ponman et al. 1999).

One way to achieve this high level of entropy is to pre-heat the gas (Kaiser 1991), and previous authors have estimated that extra non-gravitational heating of order 1 keV per (gas) particle should suffice to explain the observations. The natural choices for the heating agents are supernovae driven winds (e.g., Ponman et al. 1999) and active galactic nuclei (e.g., Yamada & Fujita 2001; Nath & Roychowdhury 2002), although uncertainties prevail in the estimates of their effects on the intracluster medium.

The other alternative is to siphon off the lowest entropy part of the gas through cooling, from the diffuse intracluster medium (ICM) to some other phase, so that it does not enter the calculations of the X-ray luminosity or X-ray weighted temperature of the gas. Voit & Bryan (2002) recently argued on the basis of the cooling function for a metallicity of $Z = 0.3 Z_\odot$ that radiative cooling can be an efficient process (given a Hubble time to operate on) in introducing an entropy floor of the appropriate level. Voit et al. (2002) have studied the effect of different kinds of entropy modifications on the properties of the cluster gas. As an example of such an entropy modification, they considered the effect of radiative cooling, assuming that it would introduce an entropy threshold corresponding to the entropy at the cooling radius (where cooling time equals the age of the system). They found that profiles

with such an entropy threshold can adequately explain the observations. Wu & Xue (2002b) also considered the effect of radiative cooling by removing the parcel of gas whose cooling time scale is less than the age of the cluster, which would cause the outer layers of gas to flow inside to again assume a hydrostatic profile. Their calculation, however, assumes that the entropy of the outer gas remains unchanged as it flows inward. Their predicted fraction of cool gas, however, exceeds the observed stellar mass fractions estimated by Roussel, Sadat & Blanchard (2000).

It is clear that radiative cooling would set the intracluster gas in motion towards the center (e.g., Silk 1976, Fabian 1994, and more recently Bohringer et al. 2002, and references therein). Since the X-ray properties of the gas mostly depend on the density and temperature profile of the gas, it is important to determine these profiles as accurately as possible, taking into account the changes brought about by such a flow.

Several authors have performed numerical simulations of cooling flows in clusters of different masses in light of the deviant X-ray properties of poor cluster, for example, Knight & Ponman (1997), Dave et al. (2002) and Muanwong et al. (2002). Knight & Ponman (1997) found that the density and temperature profiles caused by cooling flows were not sufficient to explain the X-ray properties, although they had used a $\Omega_0 = 1$ cosmology with a dark matter profile from Bertschinger (1985), different from the universal profile used by more recent authors. Also, they did not address the problem of the entropy 'floor' as it was not known then. More recently Muanwong et al. (2002) found that cooling flows which come about as a result of radiative cooling can reproduce all observations, whereas Dave et al. (2002) find some discrepancy in their results compared to the observations.

In this paper, we study simple models of cooling flows for the effect they have on the X-ray properties of clusters, and in setting up the 'entropy floor'. We simplify the cooling flow equations motivated by the recent X-ray observations (e.g., Bohringer et al. 2002). We do not have any heating sources in the flow equations, so that we can study the effect of radiative cooling alone.

We begin by setting up the background dark matter potential and the default profiles of the gas in the next section. We also introduce the cooling flow equations later in the section. We present the result of our calculations in §3 and discuss the implications, along with the uncertainties and limitations of our calculations in §4.

We assume throughout the paper that $\Omega_0 = 0.7$, $\Omega_b = 0.3$ and $h = 0.65$.

2 DENSITY PROFILE

We first consider the density profile of the dark matter which provides the potential for the gas particles.

2.1 Dark matter density profile

We assume that the gas mass is negligible compared to that of the total dark matter mass in the clusters, and that the dark matter density profile is given by the 'universal' profile, expressed in terms of a characteristic radius r_s (e.g., in Komatsu & Seljak 2002),

$$\rho_{\text{dm}}(r) = \rho_s Y_{\text{dm}}(r=r_s); \quad (1)$$

where ρ_s is a normalizing density parameter and $Y_{\text{dm}}(x)$ is given by

$$Y_{\text{dm}}(x) = \frac{1}{x(1+x)^3}; \quad (2)$$

Here the parameter α characterizes the shape of the profile. The total dark matter mass within a radius r is

$$M(r) = 4 \rho_s r_s^3 m(\alpha r/r_s); \quad (3)$$

where,

$$m(x) = \int_0^x du u^2 Y_{\text{dm}}(u) = \ln(1+x) - \frac{x}{1+x}; \quad (4)$$

Here, the last equality is valid for $\alpha = 1$ which is the much used NFW profile (Navarro et al. 1996, 1997). Recently, Moore et al. (1998) and Jing & Suto (2000) thought that $\alpha = 1.5$ better described their simulation results. For $\alpha = 1.5$, $m(x) = 2 \ln\left(\frac{p}{x} + \frac{p}{1+x}\right) - 2 \frac{q}{1+x}$ (Suto et al. 1998). The characteristic radius r_s is related to the virial radius r_{vir} by the concentration parameter c , as

$$c = \frac{r_{\text{vir}}}{r_s}; \quad (5)$$

The total mass of the cluster is assumed to be the mass inside its virial radius. The virial radius is calculated in the spherical collapse model to be,

$$r_{\text{vir}} = \frac{h}{(4-\beta)} \frac{M_{\text{vir}}}{c(z)} \frac{i_{1=3}}{c(z)} = \frac{h}{4} \frac{M_{\text{vir}}}{c^3 \rho_s m(c)} \frac{i_{1=3}}{c}; \quad (6)$$

where the second equality comes from evaluating equation (3) at the virial radius. Here $c(z)$ is the present day spherical overdensity of the virialized halo within r_{vir} at z in the units of the critical density of the universe $\rho_c(z)$. Following Komatsu & Seljak (2002), we assume a value $c(z=0) = 100$ for a cosmological model with $\Omega_m = 0.3$ and $\Omega_b = 0.07$.

We follow Seljak (2000) in adopting the approximation for c as a function of the cluster mass,

$$c = 6 \frac{M_{\text{vir}}}{10^{14} h^{-1} M}^{1.5} \quad (7)$$

The above set of equations specify the dark matter density profile given the mass of the cluster. We now turn our attention to the profile assumed by gas in these clusters.

To compare our results with observations, which usually use the radius r_{200} where the overdensity is 200, we compute in each case this radius, and present our results in its terms.

2.2 Gas density profile

Our aim is to determine the changes in the properties of the cluster which come about as a result of radiative cooling. For this we need to assume a 'default' profile of the gas and then study the changes wrought upon the profile by these processes.

We assume that the default profile is that of gas in hydrostatic equilibrium with the background dark matter potential. This does not specify the gas density profile as more constraints are needed. One choice is that the gas obeys a polytropic equation of state. This has been shown to provide an accurate description of the gas density and temperature profile for rich clusters. Recent analyses find that gas profiles in hydrostatic equilibrium with a polytropic index $\gamma = 1.2$, where pressure of the gas is related to the density as $p \propto \rho^\gamma$ describe the observations well (Markevitch et al. 1998). Since the rich clusters are thought to have been affected minimally by non-gravitational processes, these profiles provide a natural choice for the default profile. We note that this was also the approach of Wu, Fabian & Nulsen (2000).

Recently, Komatsu & Seljak (2002) have determined the solutions to the hydrostatic equilibrium equation, in the case of a polytropic gas, with the constraint that the gas profile is proportional to that of the dark matter at large radii. This physically motivated constraint limits the range of the polytropic index γ , and they find that their solutions yield values of γ within the range between 1.1 and 1.2 for clusters with masses between 10^{13} – $10^{15} M_\odot$, as found in observations. They also provide useful analytical fits for their solutions.

We adopt these profiles obtained by Komatsu & Seljak (2002) as one set of our default profiles (set A). We normalize these profiles by assuming that the ratio of the gas mass inside the virial radius to the total virial mass is constant for all clusters, and equals $f_{\text{b}} = f_{\text{m}}$. We

adopt a value of ρ_b as constrained by primordial nucleosynthesis, as $\rho_b = 0.02h^{-2}$ (Burles & Tytler 1999).

We also use another set of default profiles (set B), in which the gas density is given by $\rho_g(r) = (\rho_b = \rho_m) \rho_d(r)$, being proportional to the background dark matter density. This has been choice of several recent authors, e.g., Bryan (2000), Voit et al. (2002) and others. The temperature profile is then given by the equation of hydrostatic equilibrium,

$$\frac{dp}{dr} = -\rho_g(r) \frac{GM(r)}{r^2} : \quad (8)$$

where $M(r)$ is the total mass inside radius r . We calculate the temperature profile of the gas with the boundary condition that the pressure is zero at infinity (as in Wu & Xue (2000a)). The resulting profiles are different from that of Bryan (2000) only near the virial radius and does not affect our calculations of the X-ray properties, since we compute these properties only to an extent r_{200} , which is somewhat smaller than r_{vir} for our choice of cosmology.

As we will find in the next section, the default temperature profiles for set A and B differ substantially. The temperature profile for set A are flat in the core region, whereas those for set B decline towards the centre. The recent observations with the help of CHANDRA for the X-ray gas fraction in clusters favour the default profiles for set A, with gas fraction increasing with cluster mass (Allen, Schmidt & Fabian 2002). In contrast, the gas fraction for set B is constant by construction. Recent CHANDRA observations of temperature profiles of some relaxed clusters do show declining temperature in the very central region though, as in set B profiles (e.g., Schmidt, Allen & Fabian 2001).

2.3 Effect of cooling

If we define a cooling radius, r_{cool} as where the cooling time of the gas equals the age of the cluster, then the gas inside this cooling radius would cool rapidly. It is widely believed that in this case a cooling flow would ensue (Fabian 1994). Although it was generally believed in the last decade that cooling flows would have several phases, with gas being deposited at different radii, recent observations find that such multiphase gas occurs only at the very central region and for most of the region of the flow, one can assume it to be homogeneous (e.g., Bohringer et al. 2002, and reference therein). Also, recent observations rule out flows with very large mass flux and gas temperatures dropping to very low temperatures, unless at the very central regions, pointing towards the subsonic nature of the flows.

Motivated by these points, we simplify the fluid equations by assuming a steady, hom-

geneous and subsonic flow, in which the flow is dictated by the following equations:

$$\begin{aligned} \dot{M} &= 4\pi r^2 \rho u \\ \frac{d\rho}{dr} &= -\frac{d}{dr} \\ u \frac{d}{dr} (H + \Phi) &= n_e^2 \Lambda_N(T); \end{aligned} \quad (9)$$

where $H = \frac{5}{2} \frac{k_B T}{m_p}$ is the specific enthalpy, n_e is the electron density, $\Lambda_N(T)$ denotes the normalized cooling function in the units of $\text{erg cm}^3 \text{s}^{-1}$, and Φ is the gravitational potential. The cooling function is normalized in a way so that the total rate of cooling is given by $n_e n_i \Lambda_N(T)$ where n_i is the ion density (here we take $n_e = n_i$).

We assume a metallicity of $Z = Z_\odot = 0.3$ for the ICM that is observed in rich clusters and which has been used by all previous authors. We note here that there is a large uncertainty in the abundance measurements for the gas in poor clusters (Davis et al. 1999; Buote 2000). We use a fit to the normalized cooling function for this metallicity as calculated by Sutherland & Dopita (1993) as described in Appendix A.

If we scale the density and temperature to their values at r_{cool} , defining $T^0 = T/T_c$ (where T_c is the temperature at r_{cool}), $n^0 = n/n_{\text{cool}}$ and $x = r/r_{\text{cool}}$, also $\Phi = \Phi_{\text{cool}} - \Phi_s$, then the above equations can be cast into a set of two equations with dimensionless variables,

$$\begin{aligned} \frac{dT^0}{dx} &= -n^0 x^2 \frac{t_{fo}(T)}{t_{co}(T_c)} A \frac{(\ln(1+x) - \frac{x}{(1+x)^2})}{(x^2)^2} \\ \frac{dn^0}{dx} &= \frac{A n^0 (\ln(1+x) - \frac{x}{(1+x)^2})}{T^0 (x^2)^2} - \frac{n^0}{T^0} \frac{dT^0}{dx}; \end{aligned} \quad (10)$$

where we have assumed $\beta = 1$ for the background dark matter profile, and where

$$A = 4\pi G_s r_s r_{\text{cool}} m_p / k_B T_c \quad (11)$$

is a dimensionless quantity and is a measure of the ratio between the potential and thermal energies at r_{cool} . Here β is the mean molecular weight. If A is small, as is the case for rich clusters, then gravity is negligible and one has a constant pressure solution. In the last equation, we have defined the flow time at r_{cool} as,

$$t_{fo} = r_{\text{cool}} / u_{\text{cool}} = 4\pi r_{\text{cool}}^3 \rho_{\text{cool}} / \dot{M}; \quad (12)$$

and the cooling time at r_{cool} to be,

$$t_{co} = \frac{(5/2) n_{\text{cool}} k_B T_c}{n_{e,\text{cool}}^2 \Lambda_N(T_c)}; \quad (13)$$

2.4 Family of solutions

It is then possible to have a family of solutions for this equations for different boundary conditions. In the spirit of Nulsen et al. (1982; Appendix A), we will refer to the solution for which $T \neq 0$ as $x \neq 0$ (meaning $T \neq 0$ as $r \neq 0$) as the 'cooling eigensolution'. This boundary condition will fix the value of the ratio $\frac{t_{fo}}{t_{co}}$, which will in turn fix the value of the mass flux. The value of this ratio for the eigensolutions are of order unity as expected (Nulsen et al. 1982).

Larger values of $\frac{t_{fo}}{t_{co}}$ than these particular values would then yield solutions for which temperatures plunge to very low values at $r = r_{cool} = 0$. These profiles would give rise to X-ray holes in clusters of galaxy, and we will not study them here. Smaller values of the ratio lead to solutions for which temperatures are larger than those for the eigensolutions.

At the other extreme, there are solutions to the cooling flow equations with very small values of $\frac{t_{fo}}{t_{co}}$ corresponding to flows with very large mass flux rate. We find that the profiles for such small values differ little if one decreases this ratio below values of order 0.01. One can actually get a formal limit to the profiles by putting this ratio equal to zero in the cooling flow equations, and numerically obtained profiles tend toward these limiting profiles very rapidly below this value of $\frac{t_{fo}}{t_{co}}$. For these solutions, gas temperature is determined mainly by the gravitational potential, as in this case $T(r) / H(r) = \phi(r)$ (see also Fabian et al. 1984), especially for poor clusters where gravity is important (where A is large). Such cases correspond to flows with mass flux rates that are ~ 100 times larger than the rates for eigensolutions. We will refer to these set of limiting solutions as flows with the highest entropy and very large mass flux rates.

These two limits of the family of solutions parameterized by the ratio $\frac{t_{fo}}{t_{co}}$, or, equivalently, the mass flux rate, constrain the physical solutions of the cooling flow equations relevant for our purpose.

Gas beyond the cooling radius, r_{cool} will remain at hydrostatic equilibrium. For gas beyond this radius, we adopt the profiles as discussed in the preceding section, which allow us to calculate the extent r_{cool} and then \dot{m}_{cool} and T_c . We then use these values in equation (10) to determine the cooling eigensolution for $r < r_{cool}$.

We find that although the cooling eigensolutions are easily determined for set A profiles, the transition from the case of $T = 0$ at $r = 0$ to $T = 0$ at $r = r_{cool}$ happens over an extremely small range of values of the ratio $\frac{t_{fo}}{t_{co}}$, making it difficult to evaluate the exact eigensolution.

We have therefore used the lowest entropy profile, with the lowest temperature possible at the central region, as the eigensolutions for set B default profiles.

We perform two sets of calculations with the age of the clusters being 10^{10} and 1.5×10^{10} yr for the two sets. We have done the calculations for cluster masses for which $r_{\text{cool}}=r_{\text{vir}} \approx 0.01$ where the cooling flows could have some tangible effects on the observable properties of the gas. We have checked that the effect of cooling flows on the total X-ray luminosity is less than $\approx 20\%$ for clusters with larger masses.

3 RESULTS

3.1 Gas density, temperature and entropy profiles

We have computed the profiles for these two extreme cases for default profiles in set A and B. An example of the gas density and temperature profiles for a cluster mass of $3.5 \times 10^{13} M_{\odot}$ is shown in Figure 1, for a cooling time of 10^{10} yr. The top panels in Figure 1 show the density profiles, where the dotted lines show the default profile, the solid lines show the lowest entropy and the dashed lines show the highest entropy cases. The bottom panels show the temperature profiles for the corresponding cases.

An important difference between the set A and B cases is that the default gas temperature at a given radius in set B (in which the gas density is proportional to the dark matter profile) is smaller than in set A. This results in making the cooling radius larger for set B than in set A (as the cooling function in the relevant temperature range increases with decreasing temperature). This makes cooling flows somewhat more extensive for set B profiles. Although this is true for clusters of a given mass, the emission weighted temperature for set B profiles are smaller than those for set A profiles. Since the emission weighted temperature is the observed parameter, and not the mass, we find that for a given cluster temperature, set B profiles have cooling flows with smaller extent. We show the ratio $r_{\text{cool}}=r_{\text{vir}}$ as a function of the emission weighted temperature (see below) in Figure 2 for the two sets of default profiles and two choices of the cooling time. Curves in Figure 2 also show that the cooling flows are more extensive for lower temperature clusters as expected.

The corresponding entropy profiles are shown in Figure 3, which shows more differences between the cases set A and B. Firstly, set A profiles (with polytropic equation of state) have higher entropy to begin with (upper dotted line). This is expected from other results obtained by Komatsu & Seljak (2000) regarding the shape of the profile. They showed

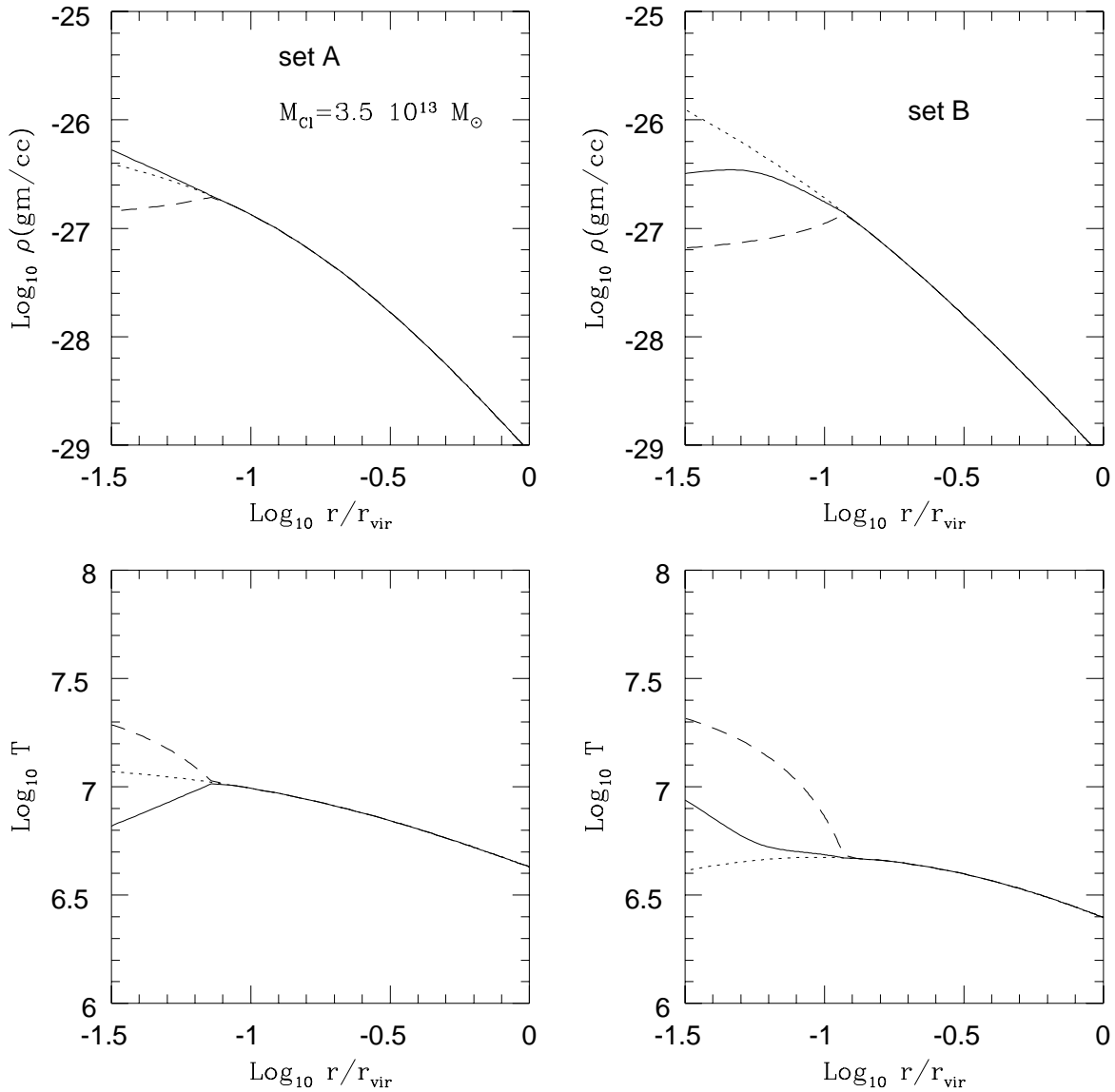


Figure 1. Gas density (top panels) and temperature (bottom panels) are plotted against $r=r_{\text{vir}}$ for cooling flows for set A (left panels) and set B (right panels) default profiles, for a cluster mass of $3.5 \cdot 10^{13} M_{\odot}$ and a cooling time of 10^{10} yr. Dotted lines in all panels show the default profile, solid lines show the profiles for the ‘cooling eigen-solutions’ and the dashed lines show the profiles with the highest mass flux rate.)

that their profiles assuming polytropic equation of state could already explain the observed relation between the parameter β (which defines the density profile). Observations show that β increases with cluster mass, showing that poor clusters have shallower profiles, which is an indication of higher entropy. It is therefore expected that these default profiles would have higher entropy than the other set of default profiles.

Secondly, cooling eigen-solutions with the lowest entropy (upper solid line) can decrease the entropy of the set A default profiles. The default profile for set B (lower dotted line), however, has very low entropy to begin with, and it is difficult to find solutions of the

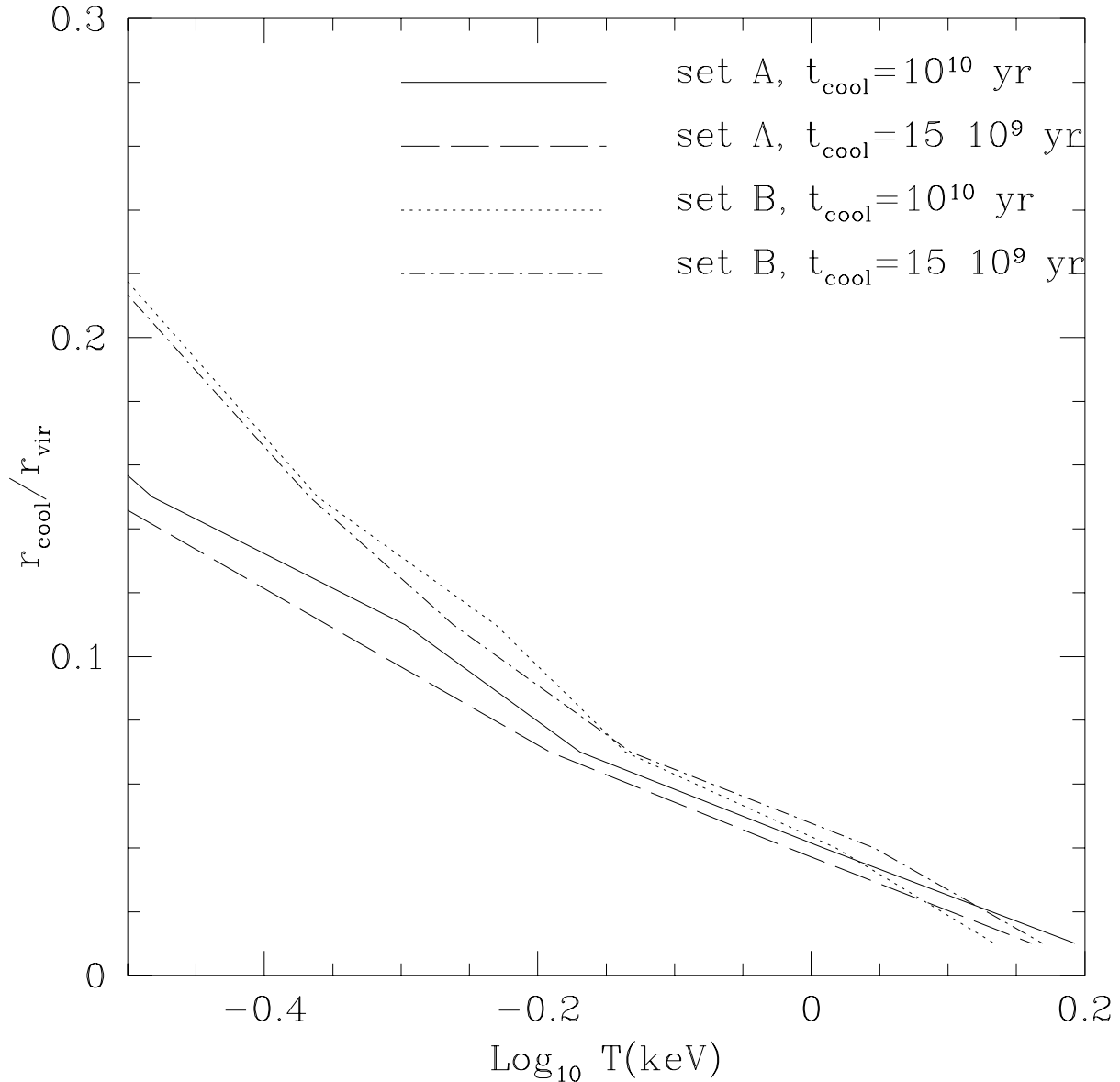


Figure 2. The ratio of the cooling radius to the virial radius corresponding to the two sets of cooling times (10^{10} and $1.5 \cdot 10^9$ yr) as a function of (emission weighted) cluster temperature.

cooling flow with entropy lower than this. The lowest entropy flows (lower solid line) in fact has larger entropy than the default profile in this case.

This difference is also manifested in the mass flux rates. Figure 4 shows the mass flux rates for the cooling eigensolutions (lowest entropy cases), with solid line for set A and dotted line for set B. Observational data points from White et al. (1997) are also shown for comparison, although we note that in light of the new measurements (see Bohringer et al. 2002) these data points may be overestimates for the mass flux. The mass flux is plotted against the emission weighted temperature (see below). As expected from our definition of

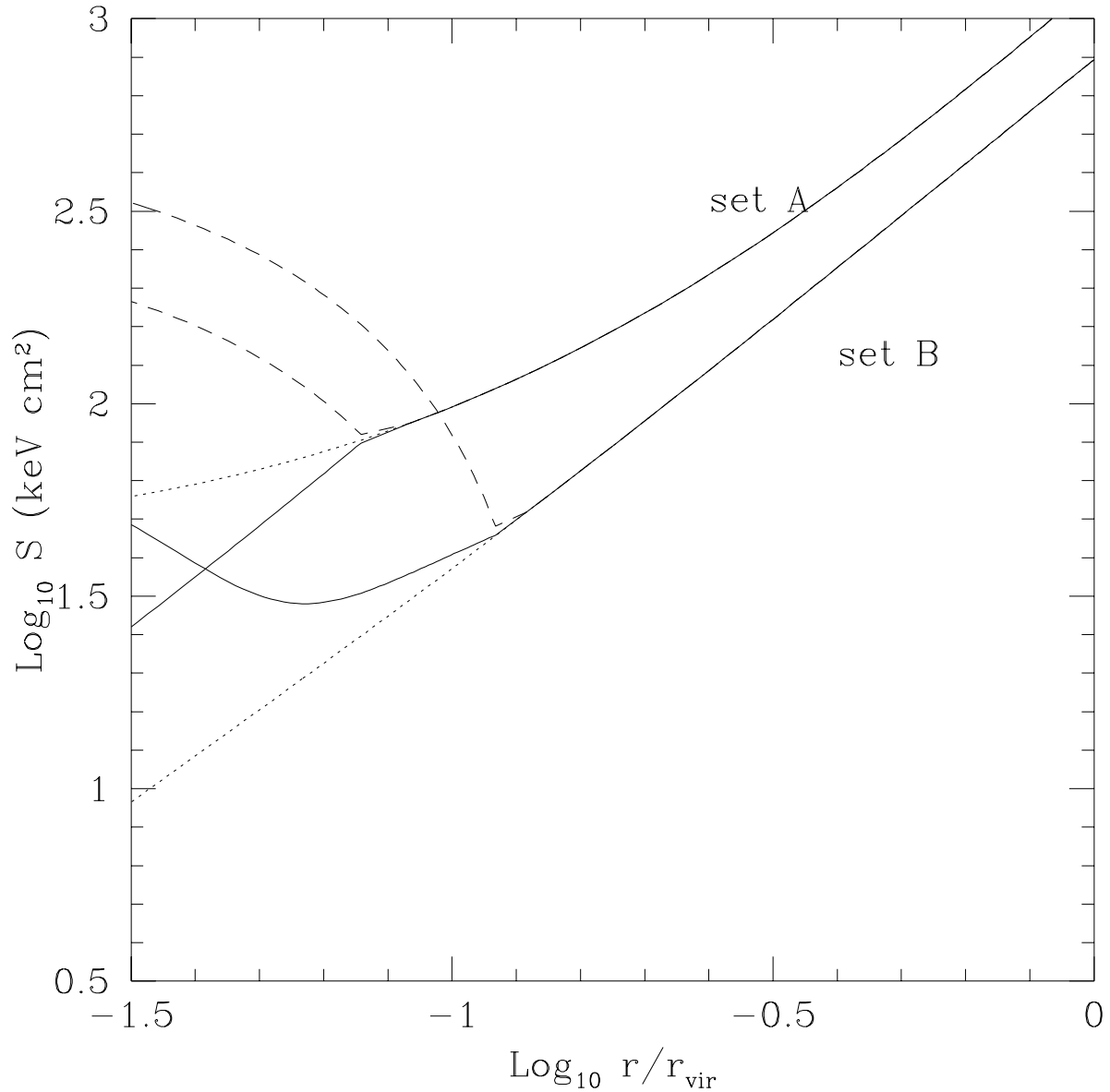


Figure 3. Entropy profiles for the cases corresponding to those in Figure 2 are shown. The upper set of curves are for set A and the lower set for set B default profiles. Dotted, Solid and long dashed lines show the entropy for the default profile, the profile for the eigensolution and the profile for the highest mass flux rate respectively.

'cooling eigensolutions', these solutions should provide the lowest mass flux rate for observed cooling flows, since flows with mass flux lower than this would correspond to holes in X-ray. The locus of these solutions for set A indeed seems to provide a lower envelope for the data points. The mass flux rate for the lowest entropy cases for set B profiles are larger than these.

Since the appropriate mass flux rate for our highest entropy flows are 100 times larger than those for the cooling eigensolutions, from the curves in Figure 4, we find that these

highest entropy flows are characterized by mass fluxes in excess of $1000 M_{\odot}$ per yr, for clusters with emission weighted temperature $T_w \approx 1$ keV.

Going back to the entropy profiles in Figure 3, the long dashed lines show the highest entropy cases. It is seen from this figure that there is a variety of entropy profiles for the gas undergoing cooling flow depending on the boundary conditions. We wish to point out that all these profiles have only one free parameter, once the default profile is given, and that is the age of the system (assumed to be 10^{10} and 1.5×10^{10} yr here). In other words, there is no single entropy threshold given the time allowed for the gas to cool, but that there is a large number of possibilities spanning a large range in entropy, depending on the mass flux.

3.2 X-ray luminosity

We compute the bolometric X-ray luminosity, and emission weighted temperature corresponding to the profiles discussed above (in the band $0.5\text{--}10$ keV), using the Raymond Smith code, for a metallicity of $Z = Z_{\odot} = 0.3$. We compute the luminosities within the dual radius r_{200} as mentioned earlier to facilitate better comparison with data, as previous authors have done. The X-ray luminosity and emission weighted temperature is computed as,

$$L_x = \int_0^{r_{200}} 4\pi r^2 n_i(r) n_e(r) \epsilon_{0.5-10} dr$$

$$T_w = \frac{\int_0^{r_{200}} 4\pi r^2 n_i(r) n_e(r) \epsilon_{0.5-10} T(r) dr}{\int_0^{r_{200}} 4\pi r^2 n_i(r) n_e(r) \epsilon_{0.5-10} dr}; \quad (14)$$

where n_i, n_e represent the ion and electron density and $\epsilon_{0.5-10}$ denotes the emissivity relevant for the $0.5\text{--}10$ keV band. We present the results in Figure 5 where the top panel shows the result for set A and the bottom panel shows the result for set B default profiles. The left panels show the results for a cooling time of 10^{10} yr and the right panels for a cooling time of 1.5×10^{10} yr. In the figure, the dotted lines again show the luminosities for the default profiles, the solid lines show the case for the eigen solutions (lowest entropy) and the long dashed lines show the case for very large mass flux rates. Dotted lines between the solid and dashed lines connect the cases of equal cluster masses. Data points from Helsdon & Ponman (2000) (filled circles) and Aumaud & Evrard (1999) (empty circles), corrected for our choice of $h = 0.65$ are also shown for comparison. The luminosities plotted here from our calculations are not 'cooling flow' corrected, since the data points are also not corrected for any possible cooling flows.

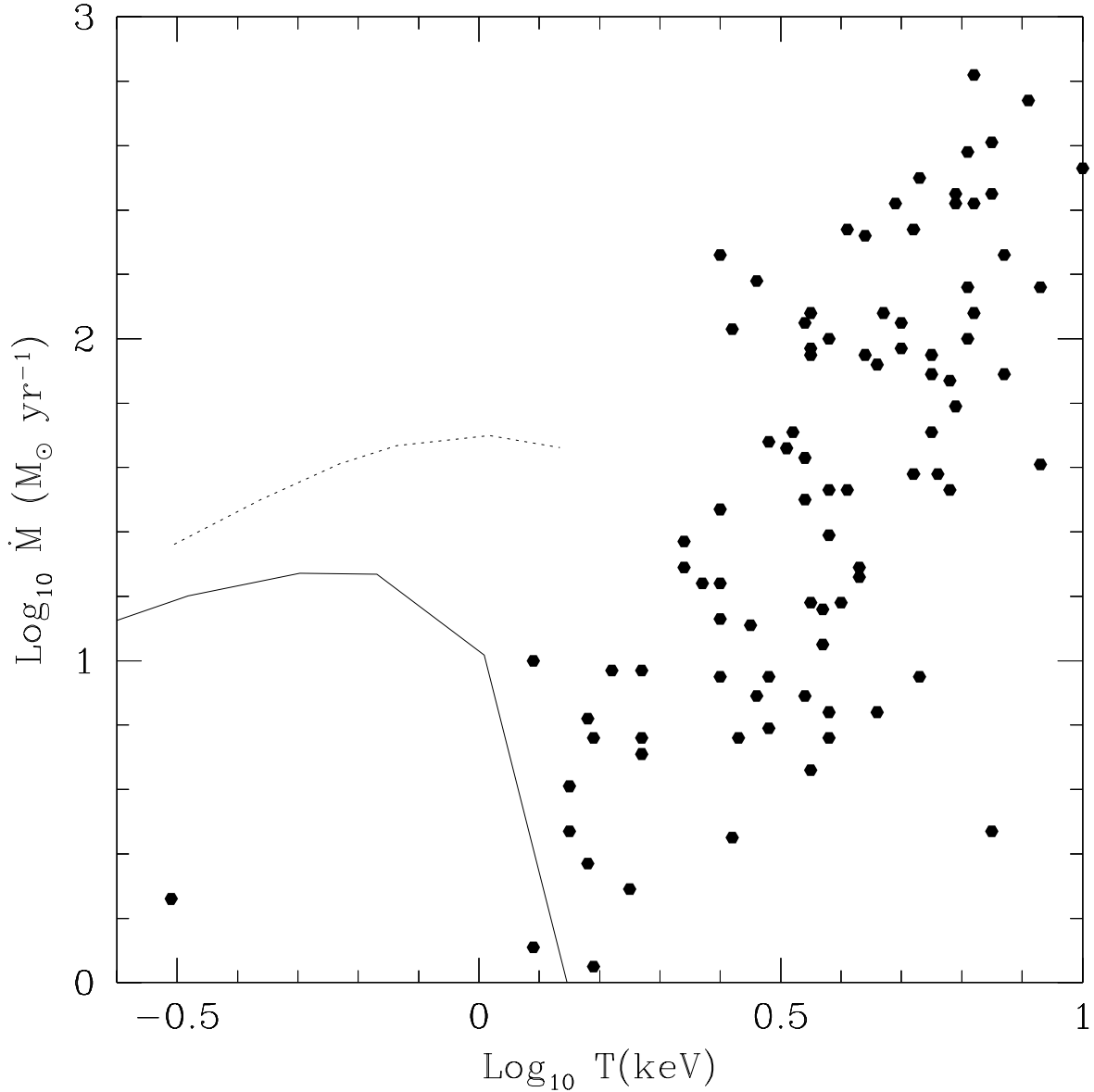


Figure 4. Mass loss rates are plotted against (emission weighted) cluster temperature for the eigen solutions for set A (solid line) and set B default profiles (dotted line), for a cooling time of 10^{10} yr. The mass losses for a cooling time of 1.5×10^{10} yr are somewhat larger than those plotted here. Data points are from White et al. (1997).

3.3 Entropy at $r = 0.1r_{200}$

We next present the values of the entropy at the fiducial radius $r = 0.1r_{200}$ in Figure 6, with results for set A in the top panel and those for set B in the bottom panel. The dotted lines in each case show the entropy for the default profile, the solid line show the case for the eigen solutions and the long dashed lines show the case of the highest entropy profiles. The dot-and-dash line shows the result of N-body simulation from Ponman, Cannon & Navarro (1999), showing the self-similar case, and the data points are also taken from this work.

Below this temperature, it is possible to raise (or even lower) the entropy level of the gas

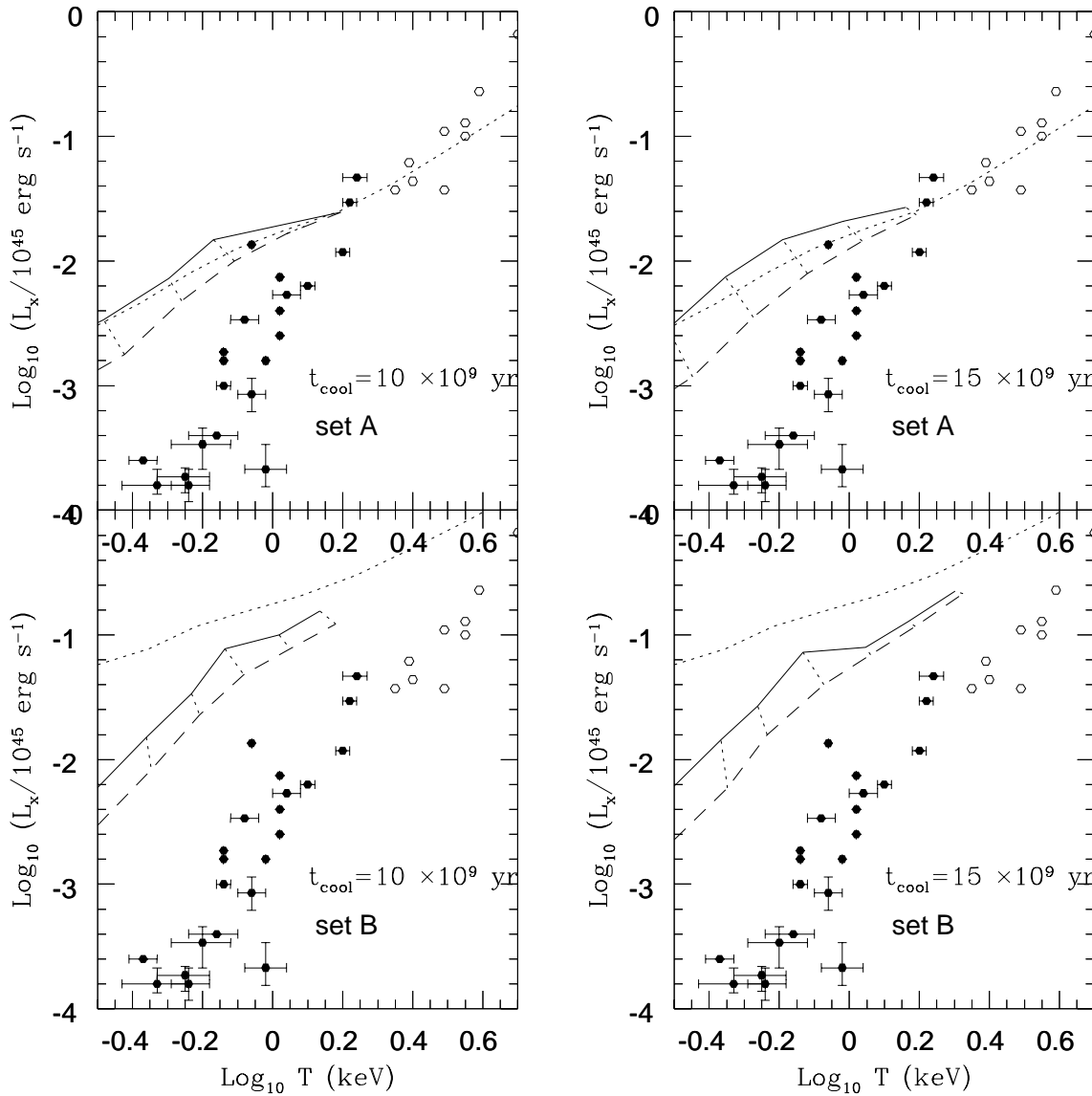


Figure 5. X-ray luminosities are plotted against the emission weighted cluster temperatures for set A (top panel) and set B (bottom panel) default profiles, for cooling time of 10^{10} yr (left panels) and 1.5×10^{10} yr (right panels). Solid, dotted and long dashed lines have the same meaning as in previous figures. Dotted lines between the solid and dashed lines connect the cases of equal cluster masses. Data points are from Helsdon & Ponman (2000) and Amaud & Evrard (1999) corrected for our choice of $h = 0.65$.

undergoing cooling flow, depending on the mass flux, and it is possible that cooling flows in very poor clusters may be responsible for raising the entropy of the gas to some extent.

4 DISCUSSION

We will discuss some of the implications of our results as well as a few uncertainties involved in our calculations in this section.

The results presented in the previous section show some of the difficulties of explaining

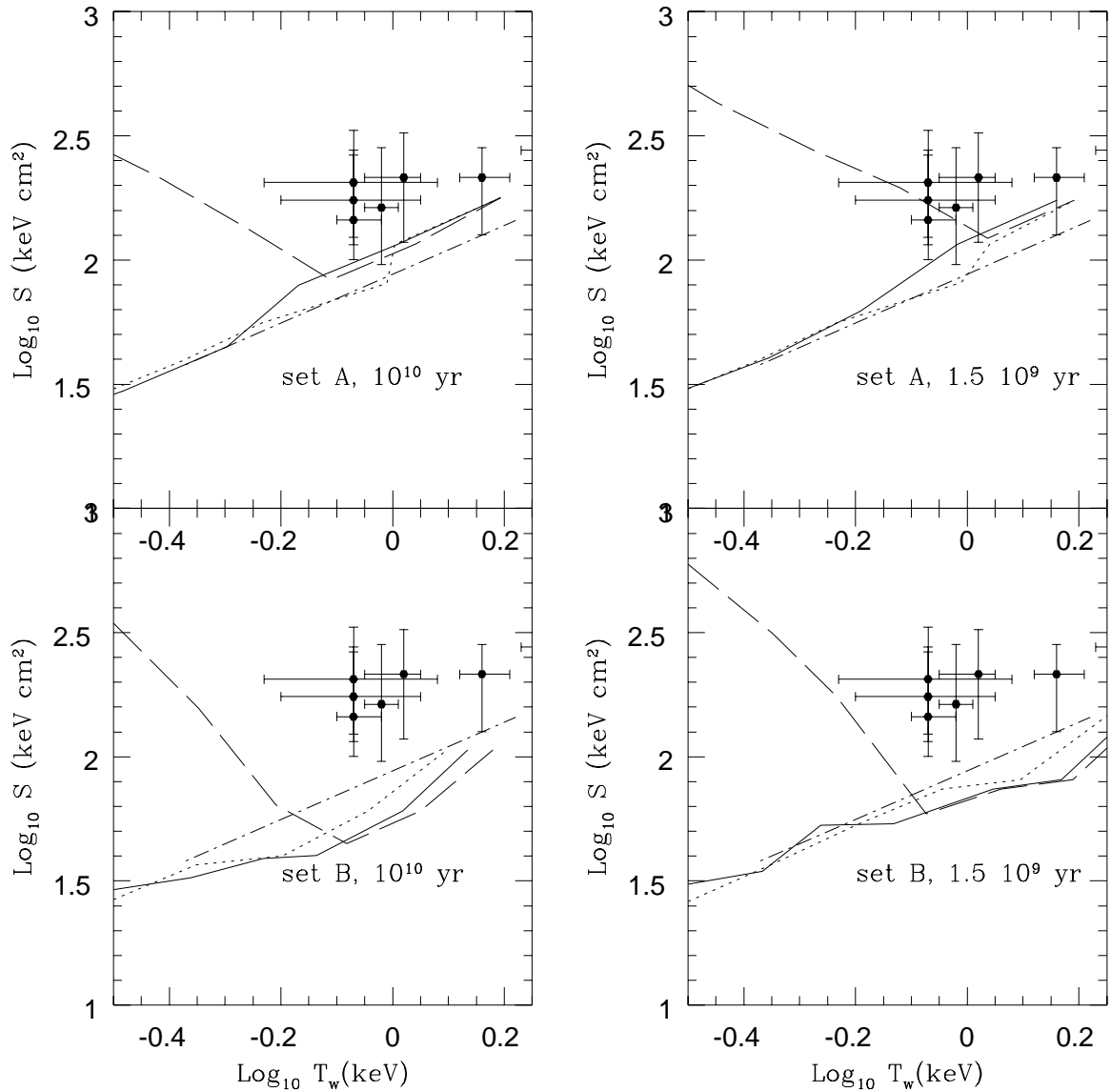


Figure 6. Entropy at $r = 0.1 r_{200}$ is plotted against emission weighted cluster temperature for set A (top panel) and set B (bottom panel) default profiles, for a cooling time of 10^{10} yr (left panels) and $1.5 \cdot 10^9$ yr (right panels). Solid, dotted and long dashed lines have the same meaning as in previous figures. The dot-and-dashed line shows the results of the numerical simulation showing the self-similar expectations, from Ponman et al. (1997).

the observations with radiative cooling alone. To recapitulate the premises of our calculations, we assumed that radiative cooling must give rise to a gas flow towards the centre. Here we have only studied steady and subsonic flows for simplicity, and motivated by the fact that recent X-ray observations do not detect flows with very high mass flux which require supersonic flows (except in the very vicinity of the centre) and also flows with mass deposition (which would make it inhomogeneous) are not detected. Let us discuss the implications of our results given these assumptions.

4.1 Entropy

Curves in Figure 6 show that the default profiles do not differ much from the self-similar case, although the set A profiles generally have larger entropy. The region bounded by the solid and long dashed lines show the possible values of entropy at $r = 0.1 r_{200}$ for cooling flows with different mass fluxes, with flows of larger mass flux rate occupying regions with larger entropy. As the curves show, these solid and dashed lines merge with the dotted line of the default profile at high temperatures. This is because of the simple reason that for high temperature clusters, the cooling radius is smaller than the fiducial radius $r = 0.1 r_{200}$, and so cooling flows do not affect the entropy measurement at this fiducial radius for high temperature clusters.

Since the entropy measurements are made at a given fiducial radius of $r = 0.1 r_{200}$, for cooling flows to have any effect on the raising of the entropy, the cooling radius must exceed this fiducial radius. We find that for both of our choice of default profiles, the cooling radius is inside this fiducial radius for $T_w = 1$ keV, for a cooling time of 10^8 yr. For a longer cooling time of 1.5×10^8 yr, the set A profiles provide a larger cooling radius, and can potentially explain the entropy measurements given the uncertainties.

Below this temperature, it is possible that cooling flows can enhance the entropy of the gas given a large enough mass flux rate (shown by the long dashed lines in Figure 6, corresponding to mass flux rates of $\sim 1000 M_\odot$ per yr). It is interesting to note that the maximum attainable entropy (at $r = 0.1 r_{200}$) is much larger than the entropy at the cooling radius (as seen from the example of entropy profile in Figure 3). The entropy at the cooling radius is obtained by setting the cooling time of the gas equal to the age of the system, as was calculated by Voit & Bryan (2002). Flow of gas under the influence of the gravitational potential can heat up the gas substantially and raise the entropy inside the cooling radius, which is clearly shown in the example portrayed in Figure 3.

4.2 X-ray luminosity

From the results in Figure 5, we find that although cooling flows decrease the luminosities to some extent, the calculated X-ray luminosities are still larger than observed luminosities. The inclusion of cooling flows decreases the X-ray luminosities to some extent for set A profiles, and to a large extent for set B profiles. This effect steepens the L_x vs. T relation compared to those of the default profiles. The lowest attainable X-ray luminosities correspond to the

long dashed lines, which show the case of flows with $(\frac{t_{\text{fo}}}{t_{\text{co}}}) = 0.01$, and with mass flux rate of $1000 M_{\odot}$ per yr. Increasing the cooling time to 1.5×10^0 yr decreases the luminosities somewhat more, but are still larger than the observed luminosities. We therefore find that flows with mass flux rates in excess of $1000 M_{\odot}$ per yr are required to explain the X-ray luminosities with radiative cooling alone.

Recently Bryan (2000) and Wu & Xue (2002a) showed that one can explain the X-ray observations by eliminating the gas in the central region (defined by the cooling region by Wu & Xue (2002b)) and replacing this gas by the outer gas, keeping the entropy constant. In reality, however, the flow that would ensue as a result of cooling flows will not keep the entropy of the gas constant, since it is not an adiabatic process. It is however possible to neglect the cooling of the gas, and therefore assume an isentropic transport of the gas, if the flow time is much smaller than the cooling time of the gas. This situation, however, corresponds to flows with very large mass flux rates, as shown by equation (12) that defines the flow time. We therefore reach the conclusion that flows with very large mass flux rates are needed to explain the observations.

4.3 Limitations

In reality the cooling radius is an increasing function of time, and the results presented above pertain to a simplified treatment of steady cooling flows, with the mass flux rate being constant in time and for all radii. One expects the mass flux rates to vary in time, as shown by the study of self-similar cooling flows by Bertschinger (1989), or the numerical simulation by Knight & Ponman (1987). Also, the cooling flows are expected to be disrupted from time to time by mergers of subclusters which would change the mass flux rate, as seen in the numerical simulation by Knight & Ponman (1987). Admittedly our simplified treatment cannot capture these aspects of cooling flows, but the conclusions reached in the previous paragraphs are expected to be general and robust.

Also, there has been a recent surge of interest in the study of cooling flows in light of the recent X-ray observations, and a number of authors have pointed out the intimate connection between active galaxies and cooling flows (e.g, Churazov et al.2001; Binney & Kaiser 2002, and references therein). For example, Binney & Kaiser (2002) pointed out that as the entropy is continually lowered by cooling flows, it will trigger some nuclear activity in the centre from time to time. They argued that this would make flows with a large drop in

temperature in the centre less probable for detection. We did not include any heating source in our cooling flow equations so that we could study the effect of only radiative cooling. In fact our results suggest that additional heating sources, possibly from active galaxies, would be needed to explain the observations.

4.4 Uncertainties

We wish to discuss some of the uncertainties pertaining to our calculations. First, there is an uncertainty of the background dark matter density profile. In the preceding sections, we have only discussed the case of the universal profile with the value of $\beta = 1$. We have also calculated the lower and upper bounds of the X-ray luminosity in the case of $\beta = 1.5$, and found that results differ only by a small amount. Recently, however, Kelson et al. (2002) have pointed out that it is even possible for the value of β to be much smaller than unity. Also, it was shown by Lloyd-Davies et al. (2002) that the choice of the concentration parameter can introduce some uncertainty in the calculations of X-ray properties of the gas. Voit et al. (2002) also showed the choice of the concentration parameter can shift the results to some extent. We based our calculations on two different sets of default profiles for these uncertainties, to determine the effects of the assumption of initial profiles on the final result. Although the details of cooling flows for our two choices of default profiles are somewhat different, the final conclusions do not differ much, suggesting that our conclusions are robust.

5 SUMMARY

We have studied cooling flow solutions for two different sets of default profiles, one with gas obeying a polytropic equation of state (set A) and the other in which the gas density is proportional to that of the dark matter (set B). We have simplified the cooling flow equations to the case of steady, homogeneous and subsonic flows. Within the purview of such flows, we find that:

(a) cooling flows can either increase or decrease the entropy of the gas compared to the default (no-cooling') profile depending on the mass flux rate. In other words, cooling for a given duration does not introduce a given entropy threshold for the gas; the entropy profile depends on the mass flux rate.

(b) For a cooling time of 10^{10} yr, the cooling radius exceeds the fiducial radius $r = 0.1 r_{200}$ only for clusters with $T_w < 1$ keV, which makes it difficult for cooling flows to have any

effect on the entropy at this radius for clusters with T_w of order of a few keV, where the expected entropy from the self-similar case falls short of the observed values. Increasing the cooling time to 1.5×10^8 yr can increase the cooling radius for clusters beyond $T_w = 1$ keV, and can potentially explain the observations. We also find that cooling flows can increase the entropy at this crucial radius for lower temperature clusters.

(c) Cooling flows that are caused by radiative cooling of gas in the central region can decrease the X-ray luminosities for poor clusters and steepen the relation between L_X and T compared to the self-similar expectation, but flows with mass flux rates in excess of $1000 M_\odot$ per yr are required to explain the observations if heating sources are not taken into account.

Acknowledgement I am indebted to Drs. Xiang-Ping Wu and Yan-Jie Xue for their gracious help with using the Raymond-Smith code. The comments of the anonymous referee which helped to improve the paper are also acknowledged with thanks.

REFERENCES

- Allen, S. W. & Fabian, A. C. 1998, *MNRAS*, 297, L57
- Allen, S. W., Schmidt, R. W. & Fabian, A. C. 2002, *MNRAS*, 334, L11
- Amaud, M. & Evrard, A. 1999, *MNRAS*, 305, 631
- Balogh, M. L., Babul, A. & Patton, D. R. 1999, *MNRAS*, 307, 463
- Balogh, M. L., Pearce, F. R., Bower, R. G. & Kay, S. T. 2001, *MNRAS*, 326, 1228
- Bertschinger, E. 1989, *ApJ*, 340, 666
- Binney, J. & Kaiser, C. 2002, preprint (astro-ph/0207111)
- Bryan, G. L. 2000, *ApJL*, 544, L1
- Borgani, S. et al. 2002, preprint (astro-ph/0205471)
- Bohringer, H., Matsushita, K., Churazov, E., Ikebe, Y. & Chen, Y. 2002, *A&A*, 382, 804
- Buote, D. A. 2000, *MNRAS*, 311, 176
- Dave, R., Katz, N. & Weinberg, D. H. 2002, preprint (astro-ph/0205037)
- Davis, D. S., Mulchaey, J. S. & Mushotzky, R. E. 1999, *ApJ*, 511, 34
- Fabian, A. C., Nulsen, P. E. J. & Canizares, C. R. 1984, *Nature*, 310, 733
- Fabian, A. C. 1994, *ARA&A*, 32, 277
- Jing, Y. P. & Suto, Y. 2000, *ApJ*, 529, L69
- Kaiser, N. 1986, *MNRAS*, 222, 323
- Kaiser, N. 1991, *ApJ*, 383, 104
- Kelson, D. D., Zabludo, A. I., Williams, K. A., Trager, S. C., Mulchaey, J. & Bolte, M. 2002, *ApJ*, in press (astro-ph/0205316)
- Knight, P. A. & Ponman, T. J. 1997, *MNRAS*, 289, 355 (KP97)
- Komatsu, E. & Seljak, U. 2002, *MNRAS*, 327, 1353
- Lloyd-Davies, E. J., Ponman, T. J. & Cannon, D. B. 2000, *MNRAS*, 315, 689
- Lloyd-Davies, E. J., Bower, R. G. & Ponman, T. J. 2002, preprint (astro-ph/0203502)
- Markevitch, M. 1998, *ApJ*, 504, 27

- McCarthy, I. G. et al. 2002, *ApJ*, 573, 515
- Muanwong, O., Thomas, P., Kay, S. T. & Pearce, F. R., 2002, preprint (astro-ph/0205137)
- Nath, B. B. & Roychowdhury, S. 2002, *MNRAS*, 333, 145
- Navarro, J. F., Frenk, C. S., White, S. D. M. 1996, *ApJ*, 462, 563
- Ponman, T. J., Cannon, D. B. & Navarro, J. F. 1999, *Nature*, 397, 135
- Roussel, H., Sadat, R. & Blanchard, A. 2000, *A&A*, 361, 429
- Schmidt, R. W., Allen, S. W. & Fabian, A. C. 2001, *MNRAS*, 327, 105
- Seljak, U. 2000, *MNRAS*, 318, 203
- Silk, J. 1976, *ApJ*, 208, 646
- Sutherland, R. S. & Dopita, M. A. 1993, *ApJS*, 88, 253
- Suto, Y., Sasaki, S. & Makino, N. 1998, *ApJ*, 509, 544
- Valageas, P. & Silk, J. 1999, *A&A*, 350, 725
- Voit, M. & Bryan, G. L. 2002, *Nature*, 414, 425
- Voit, M., Bryan, G. L., Balogh, M. L. & Bower, R. G. 2002, *ApJ*, in press (astro-ph/?)
- White, D. A., Jones, C. & Forman, W. 1997, *MNRAS*, 292, 419
- Wu, X. & Xue, Y. 2002, *ApJ*, 569, 112
- Wu, X. & Xue, Y. 2002, *ApJL*, 572, L19
- Yamada, M. & Fujita, Y. 2001, *ApJ*, 553, 145

6 APPENDIX A

We have found that the following function fits the Sutherland & Dopita (1993) cooling function for $Z=Z_{\odot} = 0.3$ very accurately, with an accuracy of 5% in the range $4.8 < \log_{10} T < 8.5$, which we have used in our calculations,

$$\begin{aligned}
 \frac{N}{10^{-23} \text{erg cm}^{-3} \text{s}^{-1}} = & 0.02 \left(\frac{T}{2 \cdot 10^6}\right)^{4.8} \left(\exp\left(\frac{T}{8.3 \cdot 10^6}\right)^4\right) \\
 & + 24 \cdot \left(\frac{T}{8 \cdot 10^6}\right) \left(\exp\left(\frac{T}{2.75 \cdot 10^6}\right)^5\right) \\
 & + 5.5 \left(\exp\left(\frac{T}{7.4 \cdot 10^6}\right)^{8.5}\right) \\
 & + 150 \cdot T^{-0.3} \left(\exp\left(\frac{T}{2.2 \cdot 10^6}\right)^8\right) \\
 & + 2.1 \left(\exp\left(\frac{T}{3 \cdot 10^6}\right)^{1.8}\right) \\
 & + 6 \cdot 10^{-7} T \left(\exp\left(\frac{T}{2.8 \cdot 10^6}\right)^7\right) \\
 & + 0.35 \left(\frac{T}{10^6}\right)^{0.4}; \tag{15}
 \end{aligned}$$

We plot this function along with the net cooling function from Sutherland & Dopita (1993) for $Z=Z_{\odot} = 0.3$, in Figure A.

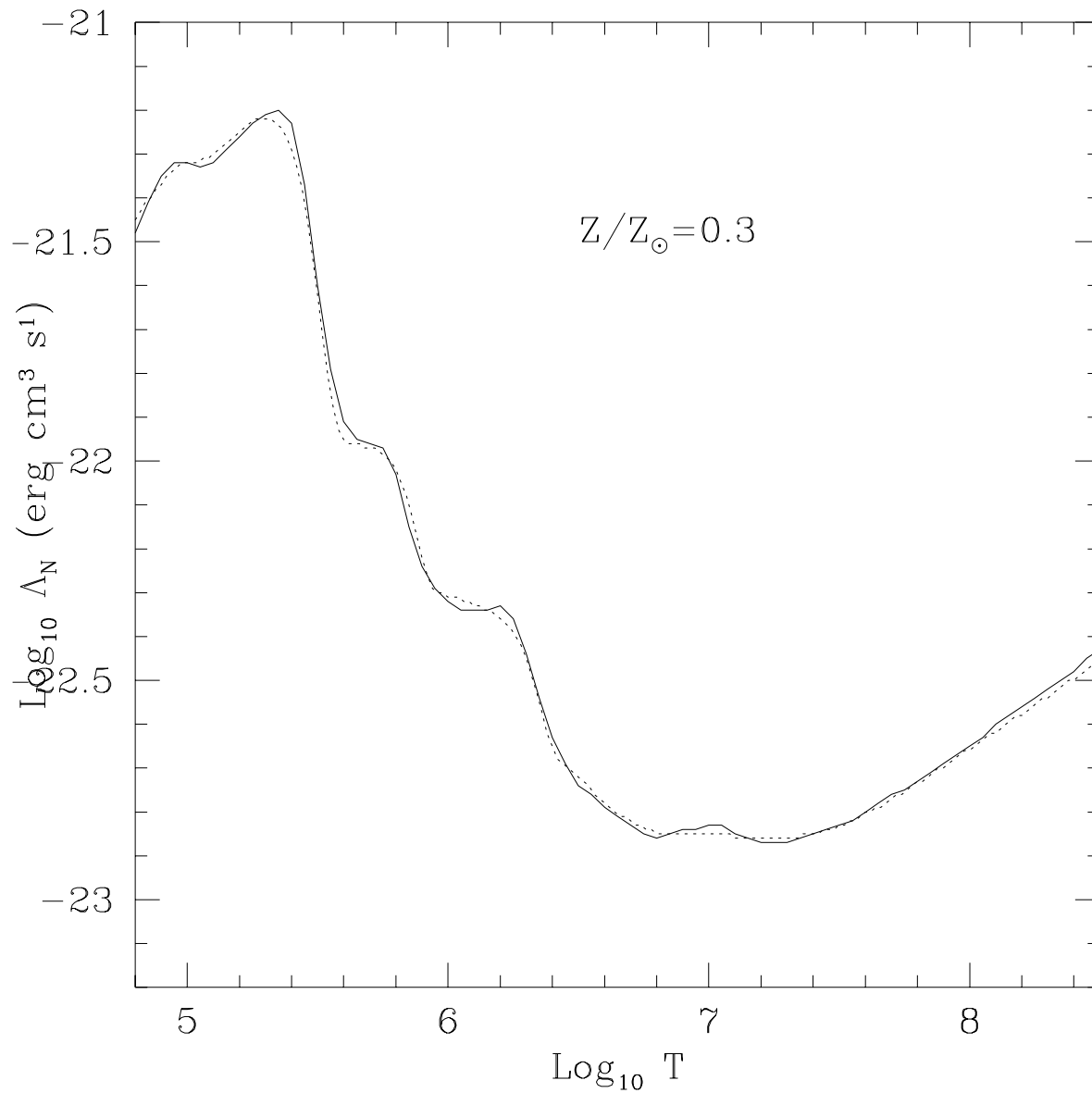


Figure 7. The cooling function of Sutherland & Dopita (1993) is shown for $Z/Z_{\odot} = 0.3$ with solid line, along with the analytical fit described here with dotted line.